

Nanomechanical displacement detection using fiber-optic interferometry

N. O. Azak, M. Y. Shagam,^{a)} D. M. Karabacak, and K. L. Ekinci^{b)}
College of Engineering, Boston University, Boston, Massachusetts 02215

D. H. Kim and D. Y. Jang
College of Engineering, Seoul National University of Technology, Seoul 139-743, South Korea

(Received 27 July 2007; accepted 7 August 2007; published online 29 August 2007)

We describe a fiber-optic interferometer to detect the motion of nanomechanical resonators. In this system, the primary technical challenge of aligning the fiber-optic probe to nanometer-scale resonators is overcome by simply monitoring the scattered light from the devices. The system includes no free-space optical components, and is thus simple, stable, and compact with an estimated displacement sensitivity of $\sim 0.3 \text{ pm}/\sqrt{\text{Hz}}$ at optical power levels of $\sim 0.75 \text{ mW}$. © 2007 American Institute of Physics. [DOI: [10.1063/1.2776981](https://doi.org/10.1063/1.2776981)]

Nanomechanical resonators or nanoelectromechanical systems¹ (NEMS) present interesting possibilities in a number of applications as well as in fundamental research. With very small masses, high frequencies, low intrinsic dissipation, and compatibility to batch fabrication, applications of these devices span from ultrasensitive mass² and force³ detection to quantum information processing.⁴

There is a relentless effort to develop efficient and sensitive transducers for NEMS.^{5–8} Optical techniques remain among the most sensitive even for the smallest devices.⁹ One usually uses free-space optical components, e.g., lenses and beam splitters, to assemble an optical detection system. The principal challenges associated with operating such systems are the stringent alignment requirements, large susceptibility to external perturbations, and the insertion loss of the optical components. Fiber interferometry, on the other hand, provides a cheap and robust alternative to free-space-based optical detection. Here, the probe laser beam is guided toward the moving surface in a fiber-optic medium. The reflected light from the moving surface is collected with the same fiber and is guided back onto a photodetector, where it interferes with a reference beam. Fiber interferometry has been used in a number of applications, such as atomic force microscopy,¹⁰ magnetic resonance force microscopy,³ and Casimir force detection.¹¹

The application of fiber interferometry to detect NEMS motion involves challenges. The principal one is approaching and aligning the fiber tip to the submicron NEMS structures. Given the size of a cleaved fiber tip, the orthogonal fiber-sample geometry and the typical fiber-sample separation, it is not practical to use an optical imaging system. Previously, fiber interferometry has been demonstrated on NEMS through the use of a fiber focuser,¹² which results in a spot size well below a micron. In this letter, we simplify and extend this approach to bare-cleaved fibers. First, we show that, it is indeed, possible to image nanoscale devices and to align the macroscopic fiber to them by simply monitoring the scattered light. Then, we study the optical displacement signal as a function of the system parameters.

A schematic of our experimental setup is shown in Fig. 1(a). The setup accomplishes two purposes: it images the sample devices for alignment and it allows high frequency displacement measurements. The main component of the interferometer is the 3 dB fiber coupler which acts similar to a beam splitter. A diode laser with wavelength $\lambda \approx 658 \text{ nm}$ and coherence length $l_c \sim 4.3 \text{ mm}$ is coupled into port 1, which splits the power evenly between ports 3 and 4. Port 3 is connected to a photodetector to monitor the laser power. The inset of Fig. 1(a) shows the bare-cleaved end of the fiber, which originates from port 4 of the 2×2 fiber coupler. To approach the bare-cleaved fiber to the NEMS chip, a three-axis translation stage is used. Parallelism between the bare-cleaved fiber and the chip surface is achieved using a tilt platform. The high frequency optical displacement signal is collected by the same bare-cleaved fiber, and carried through port 2 of the fiber coupler to a second photodetector. This photodetector is connected to the input port of a network analyzer. The nanomechanical resonators are actuated electrostatically using the oscillator output from the network analyzer.

The nanomechanical resonators used in this study are fabricated using standard techniques.⁹ The device chip is coated uniformly with a 10-nm-thick Al film for electrostatic actuation. After fabrication and wire bonding, the chip is placed on the translation stage. Imaging and alignment is accomplished by a point-by-point raster scan of the cleaved fiber tip along the sample surface. Figures 1(b) and 1(c) show scanning electron microscope (SEM) and optical images of the device area of the sample chip, respectively. Since feature depths are significantly less than the Rayleigh range and all surfaces have uniform reflectivity, we estimate that contrast in the optical images is primarily due to diffraction of light. The flat large structures appear to have uniform brightness with dark edges, while the narrow beams appear completely dark. Given that the diameter of the fiber spot is $\sim 5 \mu\text{m}$, our optical images are adequate for alignment.

Figure 2 shows resonance measurements on a doubly clamped beam of width (w) \times thickness (h) \times length (l) = $360 \text{ nm} \times 230 \text{ nm} \times 8 \mu\text{m}$, under ambient conditions. The resonance frequency and the quality factor of the out-of-plane fundamental flexural mode are $\Omega_0/2\pi \approx 35.5 \text{ MHz}$ and $Q \approx 175$, respectively. In Fig. 2(a), the incident optical power is decreased between successive frequency traces. The

^{a)}Present address: Advanced Metrology Systems, LLC, Natick, MA 01760, USA.

^{b)}Author to whom correspondence should be addressed; electronic mail: ekinci@bu.edu

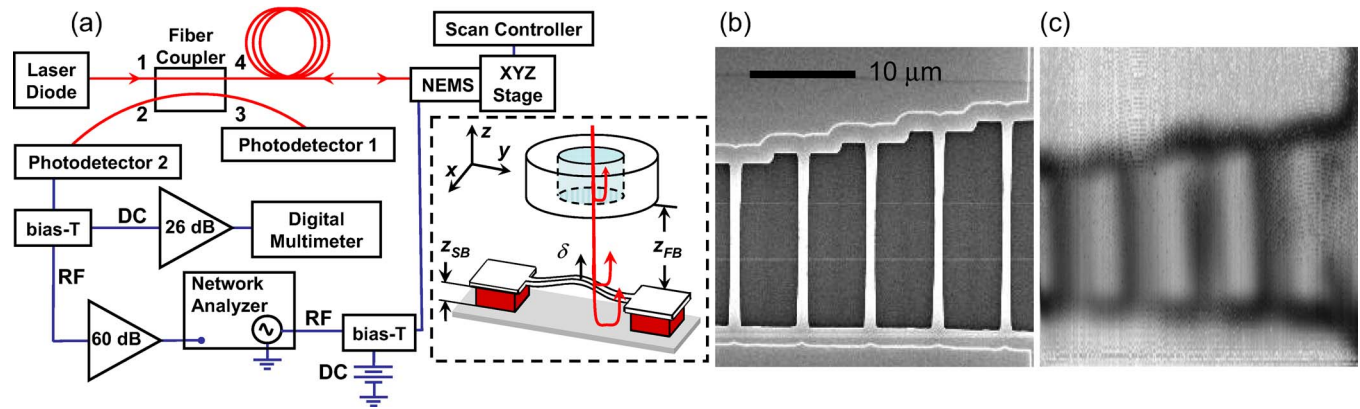


FIG. 1. (Color online) (a) Block diagram of the experimental setup. The inset shows a closeup of the fiber and the NEMS device. (b) SEM and (c) fiber-scanned image of 500 nm wide doubly clamped beams. The field of view in both images is $\approx 30 \times 30 \mu\text{m}^2$. Fiber-scanned image is obtained through a raster scan with step sizes of 100 and 250 nm along the x and y axes, respectively. The slight disagreement in the y scales may be due to the drift in the translation stage.

displacement signal amplitude is roughly linear with the incident laser power [Fig. 2(a) inset]. Figure 2(b) shows the resonant response of the same beam measured at different fiber-sample separations z_{FB} [see Fig. 1(a) inset]. To determine z_{FB} , we gently touch the fiber tip to the chip surface ($z_{\text{FB}}=0$), and then calibrate against the interference fringes formed between the light reflecting from the surface and the fiber-air interface, as z_{FB} is increased. We note that the contact with the chip surface may sometimes contaminate the cleaved fiber tip. The sign of a contamination is usually a reduction in the optical signal.

In an effort to understand the limits of displacement detection in this system, we have measured the optical spot

diameter d of the cleaved-fiber as a function of the distance between the fiber tip and the probed surface. The measurements are performed using an optical knife-edge technique¹³ on a photodetector with lithographically defined Cr patterns. Figure 3 displays the spot diameter d as a function of the separation z_{FB} between the fiber tip and the photodetector. The dashed line is a best fit to the Gaussian beam¹⁴ with $d(z_{\text{FB}})=d_0[1+(z_{\text{FB}}/z_0)^2]^{1/2}$. The beam shape with the relevant parameters is illustrated in the lower inset of Fig. 3. In the fitting, the fiber mode diameter d_0 and the Rayleigh range z_0 are taken as fit parameters and are determined to be $d_0 \approx 5.14 \mu\text{m}$ and $z_0 \approx 33.85 \mu\text{m}$. For the fiber used, the manufacturer specifications are $d_0 \approx 4 \mu\text{m}$ and $z_0 \approx 20 \mu\text{m}$. The discrepancy may be due the deformation of the fiber during the cleaving process. The upper inset of Fig. 3 shows the displacement signal amplitude as a function of the optical spot diameter. The data in Fig. 2(b) and the d vs z_{FB} function obtained from Fig. 3 (main) are used in generating the plot. As the spot becomes larger, the displacement signal goes down, indicating that it is advantageous to keep the fiber tip close to the chip.

We now turn to a simplified analysis of the displacement signal. First, due to Fresnel reflection,¹⁴ $\sim 4\%$ of the optical power arriving the cleaved end is reflected back into the

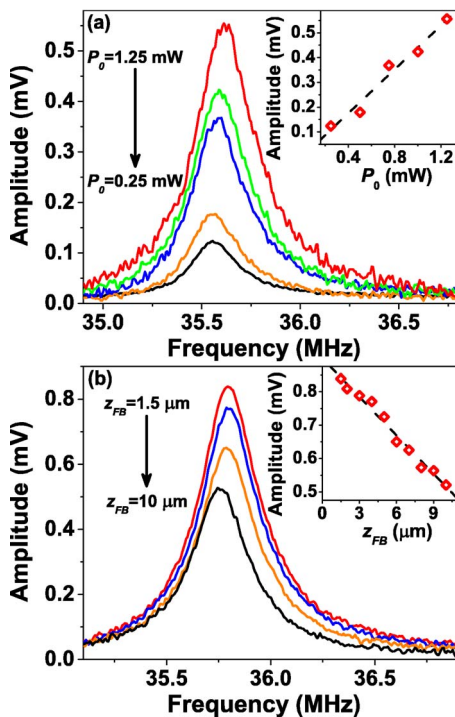


FIG. 2. (Color online) (a) Resonance of a NEMS beam with dimensions ($w \times h \times l$) $360 \text{ nm} \times 230 \text{ nm} \times 8 \mu\text{m}$, measured at varying laser power level $P_0=1.25, 1, 0.75, 0.50,$ and 0.25 mW and constant z_{FB} . The inset shows the signal amplitude as a function of P_0 . (b) Same measurement at constant $P_0=0.75 \text{ mW}$ but varying fiber-beam distance $z_{\text{FB}}=1.5, 4, 6,$ and $10 \mu\text{m}$. The inset is a plot of the signal amplitude as a function of z_{FB} . The dashed lines in both (a) and (b) are linear fits.

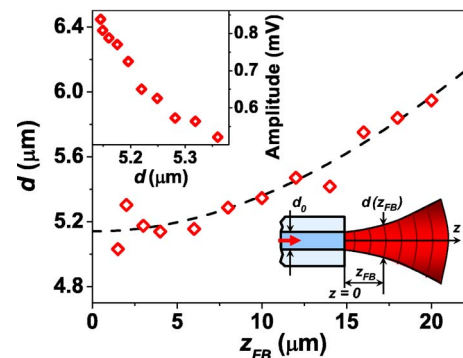


FIG. 3. (Color online) Optical spot ($1/e^2$) diameter d measured as a function of the distance z_{FB} between the cleaved end of the fiber and the surface where the spot forms. The dashed line is a fit to $d=d_0[1+(z_{\text{FB}}/z_0)^2]^{1/2}$ with $d_0 \approx 5.14 \mu\text{m}$ and $z_0 \approx 33.85 \mu\text{m}$. The lower inset is an illustration of the light exiting the fiber with the relevant parameters. The upper inset shows the displacement signal amplitude as a function of the optical spot diameter d .

fiber. The remaining light impinges upon the chip and is reflected from both the moving nanomechanical beam and the substrate below, as demonstrated in the inset of Fig. 1(a). The resulting optical power on the photodetector can be expressed as

$$P_{PD} \sim P_0 |e^{i\omega t} (\sqrt{r_f} + \sqrt{r_b} e^{-2ik_0(z_{FB}-\delta)} + \sqrt{r_s} e^{-2ik_0(z_{FB}+z_{SB})})|^2, \quad (1)$$

where k_0 is the wave number in air, δ is the (time-dependent) beam displacement and P_0 is the incoming optical power. The coefficients r_f , r_b , and r_s , respectively, represent the normalized optical power reflected from the fiber-air interface, the nanomechanical beam and the substrate, and collected back in the fiber. For instance, $r_s P_0$ is the optical power collected in the fiber reflecting from the substrate. From reflection measurements, we estimate that up to 90% of the power exiting the fiber is coupled back into it, i.e., $r_s \sim 0.9$, when the reflective surface is within $z_{FB} \sim 5 \mu\text{m}$. Note that $r_f \approx 0.04$. Since $\delta \ll \lambda$, the high frequency displacement signal can be reduced to $\sim 2k_0 P_0 \delta \sqrt{r_b} [\sqrt{r_f} \sin(2k_0 z_{FB}) - \sqrt{r_s} \sin(2k_0 z_{SB})]$. Thus, the high frequency displacement signal should only depend linearly on the incoming laser power P_0 , in agreement with the data in Fig. 2(a). In Fig. 2(b), when z_{FB} is decreased, a steady increase in the signal amplitude is observed. Given that $r_f \ll r_s$, the increase in the amplitude suggests that collection efficiency increases as the fiber tip approaches the chip.

At the optical power levels used here, the displacement sensitivity is limited by the $0.5 \text{ nV}/\sqrt{\text{Hz}}$ voltage noise in the amplifier. To estimate the displacement sensitivity of the fiber interferometer for a typical nanomechanical beam resonator, we first calibrated the absolute displacement of the resonator against the drive force in a path-stabilized Michel-

son interferometer. By using similar drive levels in the fiber interferometer, we converted the optical signal in the fiber interferometer to an absolute displacement. This exercise resulted in an estimated displacement sensitivity of $\sim 0.3 \text{ pm}/\sqrt{\text{Hz}}$ at an optical power level of $\sim 0.75 \text{ mW}$.

In conclusion, we have demonstrated a simple, robust, and sensitive fiber interferometer that can be used in the NEMS domain.

The authors acknowledge generous support from the U.S.-NSF (through Grant Nos. CMS-324416, BES-216274, and ECCS-0643178) and the Korean MOCIE.

- ¹K. L. Ekinci and M. L. Roukes, *Rev. Sci. Instrum.* **76**, 061101 (2005); H. G. Craighead, *Science* **290**, 1532 (2000).
- ²K. L. Ekinci, X. M. H. Huang, and M. L. Roukes, *Appl. Phys. Lett.* **84**, 4469 (2004).
- ³D. Rugar, R. Budakian, H. J. Mamin, and B. W. Chui, *Nature (London)* **430**, 329 (2004).
- ⁴K. C. Schwab and M. L. Roukes, *Phys. Today* **58**, 36 (2005).
- ⁵A. N. Cleland and M. L. Roukes, *Appl. Phys. Lett.* **69**, 2653 (1996).
- ⁶R. Knobel and A. N. Cleland, *Appl. Phys. Lett.* **81**, 2258 (2002).
- ⁷P. A. Truitt, J. B. Hertzberg, C. C. Huang, K. L. Ekinci, and K. C. Schwab, *Nano Lett.* **7**, 120 (2007).
- ⁸M. Li, H. X. Tang, and M. L. Roukes, *Nat. Nanotechnol.* **2**, 114 (2007).
- ⁹T. Kouh, D. Karabacak, D. H. Kim, and K. L. Ekinci, *Appl. Phys. Lett.* **86**, 013106 (2005); D. W. Carr, L. Sekaric, and H. G. Craighead, *J. Vac. Sci. Technol. B* **16**, 3821 (1998).
- ¹⁰D. Rugar, H. J. Mamin, and P. Guethner, *Appl. Phys. Lett.* **55**, 2588 (1989).
- ¹¹G. Bressi, G. Carugno, A. Galvani, R. Onofrio, G. Ruoso, and F. Veronese, *Class. Quantum Grav.* **18**, 3943 (2001).
- ¹²I. Favero, C. Metzger, S. Camerer, D. König, H. Lorenz, J. P. Kotthaus, and K. Karrai, *Appl. Phys. Lett.* **90**, 104101 (2007).
- ¹³D. Karabacak, T. Kouh, C. C. Huang, and K. L. Ekinci, *Appl. Phys. Lett.* **88**, 193122 (2006).
- ¹⁴B. E. A. Saleh and M. C. Teich, *Fundamentals of Photonics*, 1st ed. (Wiley-Interscience, New York, 1991).